Simultaneous retrieval of water vapour, temperature, and cirrus clouds properties from measurements of far infrared spectral radiance over the Antarctic Plateau

Gianluca Di Natale[1], Luca Palchetti[1], Giovanni Bianchini[1], and Massimo Del Guasta[1]

[1]Istituto Nazionale di Ottica - CNR

Correspondence to: Luca Palchetti (Luca.Palchetti@ino.it)

Abstract. The possibility to separate the contributions of the atmospheric state and of the ice clouds by using spectral infrared measurements is a fundamental step to quantify the cloud effect in climate models. A simultaneous retrieval of cloud and atmospheric parameters from infrared wide-band spectra will allow the disentanglement of the spectral interference between these variables. In this paper we describe the development of a code for the simultaneous retrieval of atmospheric state and ice clouds parameters, and its application to the analysis of the spectral measurements acquired by the Radiation Explorer Far Infrared – Prototype for Applications and Development (REFIR–PAD) spectroradiometer, which is operative at Concordia Station on the Antarctic Plateau since 2012. The code performs the retrieval with a computational time comparable with the instrument acquisition time. Water vapour and temperature profiles and the clouds optical and micro-physical properties, such as the generalised effective diameter and the ice water path, are retrieved by exploiting the 230−980 cm^{-1} spectral band. To simulate atmospheric radiative transfer, the Line By Line Radiative Transfer Model (LBLRTM) has been integrated with a specifically developed subroutine based on the δ-Eddington two-stream approximation, whereas the cirrus clouds single scattering properties have been derived from a database for hexagonal column habits. In order to detect ice clouds, a back-scattering and depolarisation lidar, co-located with REFIR–PAD has been used, allowing to infer the position and the cloud thickness to be used in the retrieval. A climatology of the vertical profiles of water vapour and temperature has been performed by using the daily radiosounding available at the Station at 12 UTC. The climatology has been used to build an a priori profile correlation to constrain the fitting procedure. An optimal estimation method with the Levenberg-Marquardt approach has been used to perform the retrieval. In most of the cases, the retrieved humidity and temperature profiles show good agreement with the radiosoundings, demonstrating that the simultaneous retrieval of the atmospheric state is not biased by the presence of cirrus clouds. Finally, the retrieved cloud parameters put in evidence correlation laws between cloud temperature and optical depth, and between effective particle diameter and ice water content. These correlations are similar to the statistical correlations measured on the Antarctic coast at Dumond D'Urville and in the Arctic region.

1 Introduction

Cirrus clouds have a strong effect on the Earth radiation budget (Cox et al., 2010; Harries et al., 2008; Kiehl and Trenberth, 1997; Liou, 1986; Lubin et al., 1998) and on the determination of the overall climate sensitivity (Baran et al., 2014; Hardiman

et al., 2015; Cox et al., 2015). However their radiative impact is still uncertain (Maestri et al., 2005; Baran, 2007; Stoker et al., 2013) since they show a very strong variability in coverage extent, altitude (Mahesh et al., 2005) as well as in the crystal size/shape distribution (Sassen et al., 2008; Baum et al., 2005a, b). As reported by Baran (2009), the Earth-atmosphere radiation balance depends upon many different parameters characterising cirrus clouds, such as geometrical thickness, particles size and shape distribution (PSD) of ice crystals and most of all the optical depth. Furthermore their coverage is still not well characterised, and spans from about 30% of the planet surface at any given time to 70% in tropical areas (Wylie and Menzel, 1999), so their climate effect could be very important.

The radiative characterisation of cirrus clouds is still uncertain due to the very complex shapes of their particles and the difficulty to detect very small crystals (De Leon and Haigh., 2007). The strongest radiative effect of cirrus occurs in the atmospheric window region ($8-12\ \mu$m) and is highly dependent on the cloud optical thickness. The contribution of the far infrared region (FIR) below 667 cm^{-1} (>15 μm) is also very important (Maestri et al., 2014) because in this region the emitted spectrum is extremely sensitive to the cloud particle effective diameter, in particular for small particle sizes ($\simeq 20-30\ \mu$m). The sensitivity to effective diameter is enhanced in the FIR because of the strong modulation of the imaginary part of the refractive index of ice (Lynch et al., 2002; Baran, 2007) which has a peak at 800 cm^{-1} and a minimum at 400 cm^{-1}.

The FIR region is also very important since it represents up to 45% percent of the entire thermal flux emitted by Earth (Harries et al., 2008), thus the flux modulation induced by clouds has important effect on the energetic balance. However, in the FIR the effect of clouds overlaps with the water vapour rotational absorption band, hence it is difficult to disentangle the two competing effects (Maestri and Holtz, 2009). Wide-band spectral measurements are essential to try to separate the atmospheric state and cloud components of the climate system (Huang et al., 2010).

The determination of cloud infrared spectral properties is even more important in polar regions since, due to lower temperatures, more of the radiation exchange happens in the FIR region and cloud contribution to the modulation of the outgoing emission is stronger, driving the polar climate (Barton et al., 2014; Choi at al., 2010; Lubin et al., 2015; Pithan et al., 2014; Scott and Lubin, 2015). Unfortunately, the lack of measurements caused by the challenging environmental conditions, especially in Antarctica, prevented the development of a reliable characterisation of cloud radiative impact (Bromwich et al. , 2012). The retrieval of cloud microphysical properties from infrared spectral measurements is therefore of great interest because it would allow to relate directly the cloud microphysics to radiative properties (Cox et al., 2014; Turner, 2005; Mahesh et al., 2001a, b).

In this paper we describe a retrieval process that uses the atmospheric emission in the spectral region between $230-980$ cm^{-1} to discriminate and evaluate simultaneously both the thermal contributions of water vapour and cirrus clouds. The process is then used for the analysis of the spectrally-resolved measurements of the atmospheric radiance performed over the Antarctic Plateau in very dry conditions. The Radiation Explorer in Far InfraRed - Prototype for Applications and Development (REFIR–PAD) spectroradiometer (Palchetti et al., 2005; Bianchini at al., 2006) is very suitable for this purpose since it is one of the few operative instruments able to detect the whole infrared atmospheric radiance between $100-1400$ cm^{-1} ($7-100\ \mu$m), covering the entire pure rotational band of water vapour in the FIR. The instrument is installed at Dome-C, in the Italian-French station of Concordia, on the Antarctic Plateau (75°06′ S, 123°20′ E) at 3233 m a.s.l., and it is acquiring atmospheric emitted radiance spectra almost continuously since December 2011, both in clear and cloudy sky conditions.

Simultaneous measurements performed by a back-scattering and depolarisation lidar (Del Guasta et al., 1993), daily radiosoundings and data from a weather station located on the roof of the Physics Shelter, where REFIR-PAD is installed, have been also used in the retrieval procedure.

Since the REFIR-PAD field campaign in Antarctica has been going on for more than four years, a very large database of spectral measurements (Palchetti et al., 2015) was collected. The development of a retrieval algorithm able to analyse the entire database will allow to perform reliable statistics about the radiative contribution of the Antarctic atmosphere and ice clouds.

The modelling of clouds is a hard problem to solve since the exact distributions of crystals size and habits are very variable, which means clouds are very inhomogeneous in space and in internal structure as well as in time. The assumption of single uniform layer is typically used to describe the radiative effect of ice cirrus clouds since these clouds are optically thin (Mahesh et al., 2001b) and the internal stratification shows a small effect on the radiative transfer, see also e.g Turner et al. (2003) and Turner (2005) where the same approximation is used. Furthermore this assumption has been verified in our specific cases, where the optical depth of cirrus clouds is less than 1.2, finding that the effect of considering the stratification produces a difference that is negligible with respect to the measurement noise.

Currently there is very little information about the statistical distribution of shapes of ice particles in polar regions, e.g. Mahesh et al. (2001b) for Antarctica and Turner et al. (2003) for the Arctic show the predominance of column particles. In particular Turner et al. (2003) showed that the typical polar habits are essentially composed by hexagonal columns with a minor fraction of droxtal for small particles. Furthermore also the single scattering models developed are very few (Fu and Liou, 1993; Fu et al., 1998; Yang at al., 2005) and not validated over the whole spectral range because of the lack of measurements in the FIR. The model developed by Fu et al. (1998) has been chosen in this analysis because it well describes clouds composed of a mixture of hexagonal columns where the shape approximates the droxtal for small size particles with aspect ratio near to 1.

The algorithm described in this work makes other assumptions to simplify and optimise the simulations. The δ-Eddington two-stream approximation has been applied to simulate the radiative transfer through the cloud layer, as considered appropriate for single layer clouds (Turner, 2005). The downwelling and upwelling radiances incident at the cloud top and bottom respectively, as well as the downward radiance propagating from the cloud to the observer, are simulated by the Line By Line Radiative Transfer Model (LBLRTM) (Clough at al., 2005) at each fitting iteration. The retrieval code is an optimal estimation based on the Levenberg-Marquardt approach (Marquardt, 1963) in which the retrieved parameters are effective particle diameter and ice water path (IWP) for the cloud and some selected points of the vertical profiles of water vapour and temperature. The a priori information is given by the seasonal climatology built using the 12 UTC daily radiosoundings, and also takes into account the statistical correlations between water vapour and temperature.

The modelling of the atmosphere in presence of ice clouds by using the single scattering properties derived from the database compiled by Fu et al. (1998) for a ice crystal mixture of hexagonal columns is described in detail in section 2. The procedure to retrieve the clouds properties and the atmospheric variables is delineated in Section 3, starting from the generation of the a priori climatological profiles and the variance-covariance matrix (VCM). The procedure to choose the atmospheric levels to be retrieved, is also explained in Section 3. Finally, in Section 5, the retrieval performance is discussed.

2 Modelling of the thermal radiance emitted by cirrus clouds

The modelling of the infrared spectral radiance emitted by the atmosphere in presence of cirrus clouds has been performed with the same approach as in the work about the fitting cloud parameters for the measurements carried out with the same instrument during Testa Grigia field campaigns in 2007 and 2011 (Palchetti et al., 2015).

The δ-Eddington two-stream approximation of the radiative transfer equation (RTE) for a thermally inhomogeneous scattering layer in case of zenith-looking configuration has been used, as suggested by Deeter and Evans (1997):

$$\begin{aligned} I_E(0) = e^{-\tau} I(\tau) + \frac{D_b}{1-\beta}(1 - e^{\tau(\beta-1)}) \\ + \frac{D_+}{1-\lambda}(1 - e^{\tau(\lambda-1)}) \\ + \frac{D_-}{1+\lambda}(1 - e^{-\tau(\lambda+1)}) \end{aligned} \tag{1}$$

where $I_E(0)$ and $I(\tau)$ are the radiances at the cloud base and cloud top, respectively. The coefficients D_-, D_+ and λ are reported in Appendix A of Deeter and Evans (1997) and depend on the upwelling and downwelling radiances and the single scattering properties of the ice particles, i.e. the single scattering albedo ω, the asymmetry factor g and the optical depth τ. The β coefficient is given, according to Fu (1991) and Fu and Liou (1993), by:

$$\beta = \frac{1}{\tau} \ln \frac{B_1}{B_0} \tag{2}$$

where B_0 and B_1 are the Planck functions calculated at the temperatures of the cloud top and bottom, respectively.

Different works were performed to parameterise the single scattering properties for the large variety of ice crystal habits as a function of the cloud micro-physics (Yang et al., 2001; Yang at al., 2005; Wiser and Yang, 1998). In this work we assume an homogeneous distribution of crystal shapes of the hexagonal column type and the approximation of a single uniform layer for the cloud vertical structure.

The single scattering coefficients depending on the micro-physical properties (D_{ge}, IWP) are given by Fu et al. (1998):

$$\begin{aligned} \tau &= \mathrm{IWP}(a_0 + a_1/D_{ge} + a_2/D_{ge}^2), \\ \tau_a &= \frac{\mathrm{IWP}}{D_{ge}}(b_0 + b_1 D_{ge} + b_2 D_{ge}^2 + b_3 D_{ge}^3), \\ g &= c_0 + c_1 D_{ge} + c_2 D_{ge}^2 + c_3 D_{ge}^3 \end{aligned} \tag{3}$$

where D_{ge} is the generalised effective diameter defined as Fu (1996):

$$D_{ge} = \frac{\int_{L_{min}}^{L_{max}} D^2 L n(L) dL}{\int_{L_{min}}^{L_{max}} (DL + \frac{\sqrt{3}}{4} D^2) n(L) dL} \tag{4}$$

D, L and $n(L)$ in Eq. (4) are the width, the maximum dimension and the size distribution of the ice crystals, respectively. The coefficients a_i, b_j and c_k in Eq. (3) are tabulated between $3-100$ μm in (Fu et al., 1998), and τ_a denotes the absorption optical depth. The single scattering albedo is obtained from the following relation:

$$\omega = 1 - \tau_a/\tau \tag{5}$$

The optical parameters are scaled according to Baran (2005) as:

$$\begin{aligned} \tau' &= (1-\omega g^2)\tau \\ g' &= g/(1+g) \\ \omega' &= (1-g^2)\omega/(1-\omega g^2) \end{aligned} \tag{6}$$

The wavenumber dependence of these parameters is shown in Fig. 1 for different values of D_{ge}. As expected, due to the wavelength dependence of the imaginary part of the refractive index of ice (Lynch et al., 2002), the particle scattering is more sensitive to the variation of the effective diameter in the FIR spectral range than in the atmospheric window between $800-980$ cm^{-1} (see also Baran (2007); Palchetti et al. (2015)). On the contrary, the maximum of extinction occurs around at $700-800$ cm^{-1}, mainly due to the effect of ice absorption.

Following Baran (2007) and Rathke and Fisher (2000), the final parameters, to be used in the radiative transfer model described in the following sections, are further scaled to take into account the gas contribution in the cloud layer yielding:

$$\begin{aligned} \tau_t &= \tau + \tau_g \\ \omega'' &= \omega' \frac{\tau'}{\tau'_t} \\ g'' &= g' \frac{\tau'}{\tau'_t} \end{aligned} \tag{7}$$

where τ_g represents the optical depth of the gases calculated using LBLRTM.

A sensitivity study has been performed to compare the different responses of radiance to atmospheric state and cirrus cloud parameter variations. We have considered a typical case simulated using climatological water vapour and temperature profiles (see Sect. 4 for more details about the used climatological profiles) and a cirrus cloud of 1 km with the bottom at 1800 m above ground and τ = 1. Figure 2 shows that a variation of 10 % in the water vapour volume mixing ratio (Q) has the same effect of a 10 μm variation in D_e in the FIR, but above 500 cm^{-1} the behaviour is the opposite. Therefore the effect of these two parameters can be discriminated in spectral measurements including both spectral regions. Moreover Figure 2 also shows that the effect of a variation in the cloud τ and D_e can be discriminated by using the FIR spectral range.

Finally we note that the temperature variation mainly affects the CO_2 spectral band with the smaller effect outside this band that is due to the indirect temperature variation that is assigned to the cloud.

3 Retrieval algorithm

The simulation of the downwelling spectral radiance at the instrument level is performed by dividing the atmosphere into 52 levels with irregular vertical resolution. The vertical resolution varies from 2 m in the first layer above the instrument, where the values and variations of the main atmospheric variables are very large, up to 1 km in the upper part of the profile, around 11 km and close to the tropopause, where the atmosphere is almost transparent. The cloud temperature is calculated from the atmospheric profile as the average between the values at the top and the bottom of the cloud, the latter two levels as supplied by the lidar measurements.

The retrieved variables are D_{ge} and the IWP for the cloud and the volume mixing ratio (VMR) of water vapour ($\mathbf{Q}$) and the temperature ($\mathbf{T}$) at selected levels of the vertical profiles. Selection of the fitting levels will be described later on in Sect. 4. The remaining levels of the vertical profiles are interpolated. The molecular species whose VMR is not fitted are supplied by climatological profiles after Remedios et al. (2007). The initial guesses for the water vapour and temperature profiles, as well as the a priori information, are obtained by the seasonal climatology described in Sect. 4. The retrieval is limited to the spectral region between 230−980 cm^{-1} where the sensitivity to the selected fitting variables is maximum (see Fig. 2).

The retrieval requires the inversion of the following equation:

$$\mathbf{y} = \mathbf{F}(\mathbf{x}) + \boldsymbol{\epsilon} \tag{8}$$

where $\mathbf{F}$ is the forward model, $\mathbf{y}$ and $\boldsymbol{\epsilon}$ are the vectors of the measurement and its uncertainty, respectively, and $\mathbf{x} = (D_{ge}, \mathrm{IWP}, \mathbf{Q}, \mathbf{T})$ is the state vector of the system composed by the cloud and the atmospheric contribution for the selected levels for the vertical profiles.

An optimal estimation approach is used for the retrieval of $\mathbf{x}$ by means of the minimisation of the cost function:

$$\chi^2 = (\mathbf{y} - \mathbf{F}(\mathbf{x}))^T \mathbf{S}_\epsilon^{-1} (\mathbf{y} - \mathbf{F}(\mathbf{x})) + (\mathbf{x} - \mathbf{x}_a)^T \mathbf{S}_a^{-1} (\mathbf{x} - \mathbf{x}_a) \tag{9}$$

where $\mathbf{x}_a$ is the vector of the a priori information that we assumed coincident with the initial guess, and $\mathbf{S}_\epsilon$ and $\mathbf{S}_a$ represent the measurement and the a priori VCMs, respectively.

The measurement VCM is calculated as follow (Ceccherini and Ridolfi, 2010):

$$(\mathbf{S}_\epsilon)_{ij} = \langle \boldsymbol{\epsilon}\boldsymbol{\epsilon}^T \rangle = \delta_{ij}(NESR_j^2 + (\sigma_F)_j^2) + \varepsilon_i \cdot \varepsilon_j \tag{10}$$

where the symbol $\langle\ \rangle$ denotes the expectation value, δ_{ij} is the identity matrix, NESR is the noise equivalent spectral radiance, and $\boldsymbol{\varepsilon}$ is the calibration error of the measurement (Bianchini and Palchetti , 2008). σ_F is the forward model error due to the uncertainties in the non fitted species and the assumption done in the description of the cloud properties. The term composed of NESR and σ_F denotes the uncorrelated statistical error, whereas the term of products $\epsilon_i \cdot \epsilon_j$ represents the correlated error

component given by the calibration uncertainty with correlation equal to 1, as derived from the Planck law of emission. The forward model error σ_F is dominated by the uncertainty on the CO_2 climatological profile, which is obtained by means of the standard deviation σ_{CO_2} of the CO_2 profile (Remedios et al., 2007) and the derivative of the forward model with respect to the CO_2 volume mixing ratio. The other non fitted atmospheric species, the single layer approximation and the choice of hexagonal columns for the cloud description have a negligible effect on the VCM compared to the measurement noise.

On the other hand the a priori VCM has been obtained as a block matrix:

$$\mathbf{S}_a = \begin{pmatrix} \mathbf{S}_{cld} & \mathbf{0} \\ \mathbf{0} & \mathbf{S}_{atm} \end{pmatrix} \tag{11}$$

where $\mathbf{S}_{cld}$ is the diagonal VCM for cloud parameters expressed as:

$$\mathbf{S}_{cld} = \begin{pmatrix} \sigma^2_{D_{ge}} & 0 \\ 0 & \sigma^2_{IWP} \end{pmatrix} \tag{12}$$

The $\mathbf{S}_{atm}$ matrix is the VCM of the atmospheric profiles in which the off-diagonal elements are not null and take into account the correlations between each fitted atmospheric level and also between temperature and water vapour profiles.

Since only a few measurements of cirrus cloud parameters in the Antarctic plateau are available, to perform a rigorous statistical analysis of the correlation between D_e and IWP and between these parameters and the atmospheric state, we have chosen not to constrain the retrieval with these a priori correlations. Therefore the off-diagonal elements of $\mathbf{S}_a$ and $\mathbf{S}_{cld}$ are set to be equal to 0. In this way, the results of the simultaneous fitting of the cloud parameters and the atmospheric state will put into evidence the existing correlation between these variables.

The standard deviations of D_{ge} and IWP in the 2x2 diagonal matrix in Eq. (12) have been set to be large enough not to be serious constraints (Turner, 2005). If $\mathbf{x} = (\mathbf{Q}, \mathbf{T})$ represents the vector of the atmospheric radiosounding of water vapour ($\mathbf{Q}$) and temperature ($\mathbf{T}$) then the $\mathbf{S}_{atm}$ can be calculated from the expectation value:

$$(\mathbf{S}_{atm})_{ij} = \frac{1}{N-1} \sum_{k=1}^{N} [(x_{ik} - \bar{x}_i)(x_{jk} - \bar{x}_j)] \tag{13}$$

where i, j are the forward model level indexes and k represents the radiosounding index. The $\bar{x}$ denotes the average profile obtained from N radiosoundings. From Eq. (13) derives that for the same index $i = j$ we find the corresponding variance.

The iterative formula (Marquardt, 1963; Palchetti et al., 2008; Bianchini at al., 2007), has been implemented by using a Levenberg-Marquardt approach:

$$\begin{aligned} \mathbf{x}_{i+1} = \mathbf{x}_i + [\mathbf{K}_i^T \mathbf{S}_\epsilon^{-1} \mathbf{K}_i + \gamma \mathbf{D}_i + \mathbf{S}_a^{-1}]^{-1} \times \\ \{\mathbf{K}_i^T \mathbf{S}_\epsilon^{-1} (\mathbf{y} - \mathbf{F}(\mathbf{x}_i)) - \mathbf{S}_a^{-1} [\mathbf{x}_i - \mathbf{x}_a]\} \end{aligned} \tag{14}$$

where $\mathbf{x}_i$ is the vector state at the i-th iteration, γ is the regularization factor and $\mathbf{D}_i$ is the diagonal matrix (Gavin, 2015):

$$\mathbf{D}_i = \text{diag}(\mathbf{K}_i^T \mathbf{S}_\epsilon^{-1} \mathbf{K}_i) \tag{15}$$

and the matrix $\mathbf{K}_i$ is the Jacobian at the i-th iteration given by:

$$K_{ijl} = \frac{\partial F_j(\mathbf{x}_i)}{\partial x_l} \tag{16}$$

The values of the $\mathbf{K}_i$ matrix is determined by means of a finite difference calculation for i = 0 and in case of an increasing χ^2, while in case of a decreasing χ^2 and every $2n$ iterations (with n number of parameters), by using the Broyden rank-1 update formula (Broyden, 1965) for the quasi-Newton method:

$$\mathbf{K}_{i+1} = \mathbf{K}_i + [(\mathbf{F}(\mathbf{x}_{i+1}) - \mathbf{F}(\mathbf{x_i}) - \mathbf{K}_i \Delta \mathbf{x}_i) \Delta \mathbf{x}_i] / (\Delta \mathbf{x}_i^T \cdot \Delta \mathbf{x}_i) \tag{17}$$

with $\Delta \mathbf{x}_i = \mathbf{x}_{i+1} - \mathbf{x}_i$.

The VCM of the state vector $\mathbf{x}$ is provided by the optimal estimation as follow (Rodgers, 2000):

$$\mathbf{S}_x = (\mathbf{K}^T \mathbf{S}_\epsilon^{-1} \mathbf{K} + \mathbf{S}_a^{-1})^{-1} \tag{18}$$

The upwelling and downwelling radiances incoming at the cloud bottom and top respectively, are simulated at each iteration. The obtained values are used for the calculation of the λ, D_- and D_+ coefficients in Eq. (1). For the simulation of the upwelling radiance, the emissivity of the surface is set to be equal to 1 and the ground temperature equal to the value measured by the Vaisala station placed on the roof of the physics Shelter.

4 Climatology and optimisation of the retrieved state vector

A study of the climatology of water vapour and temperature profiles has been performed using the whole radiosoundings dataset available for the year 2014 to calculate seasonal averages, shown in Fig. 3, and standard errors. In the right panel of Fig. 3 we can note the strong temperature inversion which occurs at about 500 m above ground in Winter and Autumn, a peculiar characteristic of the Antarctic atmosphere: in these conditions the ground mean temperature can reach values below -60 °C. The water vapour VMR profiles also manifests a strong inversion in Winter and Autumn as shown in the left panel.

The standard deviation σ of the climatological profiles is used to calculate the a priori VCM. The limits of the retrieval domain are set to $\pm$ 3-σ in order to take into account the profile variability. Only for the ground level larger limits of (-200,+300) K and (1,3000) ppmv have been chosen for temperature and VMR, respectively. This is due to the much larger variability of the very first layer, that corresponds to the internal environment of the Physics Shelter. These limits represent the real physical domain in which the atmospheric variables can be varied by the retrieval routine.

In order to determine how many degrees of freedom represent at best the atmospheric states and to set the retrieval levels, a study of the matrix $\widetilde{\mathbf{K}}$ given by:

$$\widetilde{\mathbf{K}} = \mathbf{S}_y^{-\frac{1}{2}} \mathbf{K} \mathbf{S}_a^{\frac{1}{2}} \tag{19}$$

has been performed by means of the singular value decomposition (SVD):

$$\widetilde{\mathbf{K}} = \mathbf{Q} \mathbf{\Sigma} \mathbf{V}^T \tag{20}$$

The analysis has been performed by using the four seasonal climatological profiles, as shown in Fig. 3, interpolated on a grid with a vertical resolution of 100 m to calculate the Jacobians with respect to the atmospheric variables in clear sky conditions. The columns of $\mathbf{V}$ represent the eigenvectors of matrix $\widetilde{\mathbf{K}}\widetilde{\mathbf{K}}^T$ in the state space transformed by $\mathbf{S}_a^{-\frac{1}{2}}$ and to come back to the original state space we can transform the vectors by means of $\mathbf{S}_a^{\frac{1}{2}}$ (Rodgers, 2000), such that:

$$\mathbf{S}_a^{\frac{1}{2}} \widetilde{\mathbf{v}}_i = \mathbf{v}_i - \mathbf{x}_a \tag{21}$$

where $\widetilde{\mathbf{v}}_i$ are the columns of matrix $\mathbf{V}$.

As shown by Rodgers (2000) the singular values of $\widetilde{\mathbf{K}}$ perfectly represent the signal to noise ratio, and the number of singular values which are about or greater than unity represents the effective rank of the system. The singular values greater than unity correspond to the states which carry information about the parameters to be retrieved, indeed the lower ones don't bring information but only noise. Figure 4 shows that our measurement system has about 3 degrees for water vapour and 6 for temperature. The singular values also give the sensitivity to measure a singular vector (Rodgers, 2000). To avoid the oscillation in the retrieval, due to the strong variability in the lowest layers, only the singular vectors which can be measured with a sensitivity greater than about 10% of the maximum value have been taken into account in our analysis. These correspond to the first two eigenvectors for water vapour and the first three for temperature for all the seasons as shown in Fig. 4. In Fig. 5 are shown, as an example, the first three back-transformed singular vector of $\widetilde{\mathbf{K}}$ for water vapour and temperature obtained by using the winter climatology.

The retrieval levels have been set by selecting a first point at ground in order to correctly keep into account the effect of the very first atmospheric layers that are affected by the presence of the shelter and the instrument itself. Two other fitted temperature levels are set at about 10 and about 300 meters and above the ground to take into account the strong gradient in the first layers. For water vapour, other than the ground level point, another fitting point at 200 meters above ground has been chosen to correctly rescale the humidity profile in the atmosphere above the layers that are influenced by the shelter. The grid levels of water vapour and temperature profiles are interpolated between the fitted levels (linearly for temperature and logarithmically for water vapor), while the portion of the profile above the upmost fitted level is scaled according to the upmost fitted value.

5 Data selection and results

The measurements of the downwelling spectral radiance used in this work were performed from the Antarctic station Concordia by the REFIR-PAD spectroradiometer (Palchetti et al., 2015), and covered the 100–1400 cm^{-1} spectral range with a 0.4 cm^{-1} resolution. Each spectrum is the average of about 5 min of atmospheric observations. The measurement is repeated every 12 min due to the instrument calibration cycle. The instrument operates with a duty cycle of about 5 hours out of 7 to allow for pre-analysis and data transfer to Italy.

To evaluate the performances of the developed retrieval algorithm, we have selected exclusively measurements performed in presence of ice clouds and in a coincidence as close as possible with the radiosoundings routinely performed from Concordia at 12 UTC using Vaisala RS92 radiosondes. The cloud phase has been identified by analysing the logarithmic range corrected signal (RCS) and the depolarisation component provided by the lidar every 10 min. We identified 15 cases in which the above mentioned requirement were fulfilled in 2014. For each case we selected the three atmospheric spectra measured in presence of cirrus that were in better temporal coincidence with the radiosounding.

In Fig. 6 colour maps of the RCS and depolarisation signals detected by the lidar in coincidence with 4 of the selected REFIR-PAD measurements, one for each season, are shown. The red solid lines in the panels indicate the exact time of the REFIR-PAD acquisitions. Panel (a) shows the passage on 12 February 2014 of an ice cloud at 1.8 km of height with a geometrical thickness of about 1.4 km. The ice cloud in panel (b) occurred on 2 April 2014 at about 0.6 km of height with 1.4 km of thickness. Panel (c) shows the passage of an ice cloud on 10 August 2014 at 1 km with 2 km of thickness. Finally panel (d) shows a cloud at 1.6 km with 0.7 km of thickness on 1 October 2014. The depolarisation signal confirms the presence of ice in the clouds, and allows to exclude the cases of mixed-phase clouds, often occurring in polar atmospheres (Turner, 2005; Turner et al., 2003; Pithan et al., 2014; Scott and Lubin, 2015).

Figure 8 shows the fitting results for the 4 selected cases of Fig. 6, taking only the measurements closer to the 12 UTC radiosounding. The measurements (black line) are compared with the synthetic spectra (red line) obtained by the fit. The fitting residuals are shown as a green line in the bottom of the plots. Panel (a) shows the atmospheric spectrum with an ice cloud composed of large size particles, the retrieval provided 47 μm of D_{ge}, and with an optical depth of 0.4. Panels (b) to (d) correspond to ice clouds with smaller diameters, respectively 34, 21 and 23 μm, and optical depths of 0.5, 1.1 and 0.6.

The comparison between the retrieved water vapour and temperature profiles with the radiosounding, in the 4 cases considered in Fig. 6, are presented in Fig. 9. As we can see the retrieved profiles generally agree with the radiosoundings measurements. Due to the low vertical resolution of the retrieval procedure, shown by the SVD analysis, it is not possible to capture the fine vertical structures visible in the radiosounding, e.g. the sharp variations occurring around 1000 m on October 1st, 2014. Moreover, the lowermost fitted temperature point is not shown in figure for the temperature due to several biases affecting its value:

1. the strong atmospheric variability occurring in the boundary layer;

2. the fact that the radiosonde is launched at about 500 m from the shelter where REFIR-PAD is located;

3. the presence of a very strong gradient in the first 3 meters of line of sight, that include the transition between the inside of the shelter, and the outside environment.

On the other side, above 5000 m, near the tropopause level, the downwelling spectral radiance has a negligible sensitivity to atmospheric water vapour and temperature, as shown by the SVD analysis (see Fig. 5).

In order to have an indication of the quality of the results in all the analysed cases, in Fig. 10 the retrieved precipitable water vapour (PWV) and the temperature of the inversion layer are compared with the corresponding values given by the radiosonde profiles in the top and middle panels, respectively. The temperature of the inversion layer T_{13m}, corresponding to the fitted level at 13 m above ground is compared with the average temperature of the first 50 meters above ground obtained by the radiosondes in order to take into account for the fact that the forward model used in the fitting process has a finite vertical resolution. The bottom panel shows the time difference between the retrieved measurements and the closed radiosonde profile.

Figure 10 shows a general good agreement between retrieved values and radiosoundings, with the largest differences occurring when the measurements are in a less strict coincidence with the radiosonde launch and there is significant atmospheric variability, as can be seen in January, where the delay between REFIR-PAD measurements and radiosounding is about 2 hours, and atmospheric state varies significantly (the three corresponding fitting results differ). Another condition in which we can expect some differences is in wintertime, when the strong thermal inversion near ground affects the retrieval process capabilities.

The fitting results for the cirrus cloud optical and micro-physical properties are plotted as a function of time in Fig. 11 together with the cloud geometrical parameters inferred from the lidar measurements. The retrieved effective particle diameters D_e vary between 20 and 90 μm with an error lower than 20 %, with the higher uncertainties corresponding to shallow clouds with a thickness of about 300-500 m. The optical depths τ, calculated from the retrieved IWP by means of Eq. (3), are between 0.05 and 1.1. The errors, obtained through propagation from the retrieval error of the IWP, are less than 20 %. The cloud temperature T_c, corresponding to the mean temperature between cloud top and bottom, is between -30 and -60 °C. T_c is obtained from the retrieved atmospheric profile using the cloud bottom height z_b and the thickness Δz provided by the lidar, parameters that are also shown in the bottom panel of Fig. 11. We can see as the largest particle diameters occur in summer when temperature is higher, as expected from the ice particle formation process, and the optical depths are generally lower than 1, hence the analysed cirrus clouds are optically thin (Mahesh et al., 2001b; Kahn et al., 2014). The retrieved cloud temperature is, in most cases, lower than -40 °C, that is consistent with the single phase of particles as detected by the lidar.

In order to have a first qualitative evaluation of the cloud parameter retrieval performances, we have also compared the retrieved values distributions with the corresponding statistical distributions measured on the Antarctic coast at sea level at the Dumont D'Urville Station and in the Arctic. Specifically, the retrieved cloud parameters were compared with two statistical correlations where τ is related to T_c and D_e to the ice water content (IWC). The first relationship is represented by an expo-

nential function obtained from the data acquired at Dumont D'Urville in 1993 (Del Guasta et al., 1993) for cirrus clouds with temperature lower than -30 °C and is given by:

$$\tau = exp(a \cdot T_c + b) \tag{22}$$

where $a = 0.0284$ and $b = 0.2110$.

The second relation correlates the effective diameter D_e with the IWC through a logarithmic relation given by (Liou, 2008):

$$D_e = exp(a + b \cdot ln(IWC) + c \cdot (ln(IWC))^2) \tag{23}$$

where a = 4.8510, b =0.33159 and c = 0.026189 are the coefficients obtained for the Arctic region. To compare with our data, the values of IWC are calculated from the retrieved IWP, reminding the assumption of single uniform layer, as follow:

$$IWC = \frac{IWP}{\Delta z} \tag{24}$$

where Δz is the geometrical thickness of the cloud.

The relationships of Eq. (22) and (23) were used to fit the retrieved data varying the a, b, c coefficients, obtaining for the $T_c - \tau$ case $a = 0.0212$ and $b = 0.0267$, and for the IWC $- D_e$ case $a = 4.129$, $b = 0.3046$, and $c = 0.04591$.

The results of Fig. 12 show that the retrieval accuracy allows to infer distribution laws for the retrieved cloud parameters that are compatible with analogous statistical distributions. A multi-year analysis over the full dataset of our measurements is under study in order to better quantify these distribution laws.

6 Conclusions

In this work an efficient code to perform the simultaneous retrieval of the atmospheric water vapour and temperature profiles and of the cloud parameters such as the generalised effective diameters and the ice water path has been developed. The code has been applied to the analysis of the measurements performed over the Antarctic Plateau in 2014 by the REFIR-PAD Fourier transform spectroradiometer. Acquired spectra have been analysed in the 230−980 cm^{-1} spectral range. The region below 667 cm^{-1} in particular appears to be very important due to the strong modulation of the spectrum given by the presence of clouds allowing for a high sensitivity to ice particles size.

The modelling of the atmosphere has been performed by integrating the LBLRTM atmospheric forward model with a specifically developed code based on the δ-Eddington two-stream approximation of the radiative transfer to take into account for the effect of clouds. A preliminary optimisation of the retrieved state vector has been performed by means of the Jacobian matrix to set the best retrieval grid for water vapour and temperature profiles. A climatology study has been also performed by using daily radiosoundings available at Concordia Station to provide good a priori information of the atmospheric variable

correlation. Clouds and ice detection is provided by the back-scattering/depolarisation lidar installed at Concordia, near to the REFIR-PAD instrument.

The fitting procedure allows to obtain a general agreement between measurements and simulations, with the residual differences generally falling within measurement noise over the whole relevant spectral range, including the FIR. The atmospheric retrieved profiles of water vapour and temperature follow the available simultaneous radiosoundings, whereas the retrieved cirrus cloud parameters follow analogous statistical distributions available for polar regions.

This work has shown the capability to perform a simultaneous retrieval of the atmospheric state and the cloud parameters from spectral measurements of the DLR over the Antarctic Plateau. Taking into account the whole spectral range in which the cloud infrared emission is relevant, it allows to disentangle the spectral interference between the variables. This process results in a better characterisation of the ice clouds radiative properties, and will enable us to improve our understanding of their role in the Earth radiation budget.

Acknowledgements. The deployment of REFIR-PAD in Antarctica was supported by the Italian National Program for Research in Antarctica PNRA (Programma Nazionale di Ricerche in Antartide) under the following projects: 2009/A04.03, 2013/AC3.01, and 2013/AC3.06. The authors are gratefully to the research group of the Institute of Applied Physics (CNR-Florence) composed by Bruno Carli, Simone Ceccherini, Marco Gai, Samuele Del Bianco, Ugo Cortesi, Marco Ridolfi, Piera Raspollini, Flavio Barbara, for the precious and fruitful discussions.

References

Baran A. J., The dependence of cirrus infrared radiative properties on ice crystal geometry and shape of the size-distribution function, Q. J. R. Meteorol. Soc. (2005), 131, pp. 1129–1142.

Baran A. J., The impact of cirrus microphysical and macrophysical properties on upwelling far infrared spectra, Q. J. R. Meteorol. Soc., 133, 1425–1437 ,2007.

Baran A. J., A review of the light scattering properties of cirrus, Journal of Quantitative Spectroscopy and Radiative Transfer, Volume 110, 1239–1260, 2009.

Baran A. J., Hill P., Furtado K., Field P., Manners J., A coupled cloud physics–radiation parameterization of the bulk optical properties of cirrus and its impact on the Met Office Unified Model Global Atmosphere 5.0 configuration J. Climate, 27 (20), 7725–7752, 2014.

Barton N. P., Klein S. A., and Boyle J. S.: On the Contribution of Longwave Radiation to Global Climate Model Biases in Arctic Lower Tropospheric Stability. J. Climate, 27, 7250–7269, 2014, doi: 10.1175/JCLI-D-14-00126.1

Baum B.A., Heymsfield A.J., Yang P. and Bedka S.T.: Bulk scattering properties for the remote sensing of ice clouds. Part I: Microphysical data and models, Journal of Applied Meteorology, 44(12), 1885–1895, 2005.

Baum B.A., Yang P., Heymsfield A.J., Platnick S., King M.D., Hu Y. and Bedka S.T.: Bulk scattering properties for the remote sensing of ice clouds. Part II: Narrowband models, Journal of Applied Meteorology, 44(12), 1896–1911, 2005.

Bianchini G., Palchetti L., Carli B.: A wide-band nadir-sounding spectroradiometer for the characterization of the Earth's outgoing long-wave radiation, Proc. SPIE, 6361, 2006.

Bianchini G., Palchetti L.: Technical Note: REFIR-PAD level 1 data analysis and performance characterization, Atmos. Chem. Phys., 8, 3817–3826, doi:10.5194/acp-8-3817-2008, 2008.

Bianchini G., Carli B.,Cortesi U.,Del Bianco S.,Gai M.,Palchetti L.: Test of far-infrared atmospheric spectroscopy using wide-band balloon-borne mmeasurements of the upwelling radiance,Journal of Quantitative Spectroscopy & Radiative Transfer 109 (2008) 1030–1042.

Birch K. P. and Downs M. J.: Correction to the Updated Edlén Equation for the Refractive Index of Air, Metrologia, Vol.31, No. 315, 1994.

Bromwich D. H., Nicolas J. P., Hines K. M., Kay J. E., Key E. L., Lazzara M. A., Lubin D., McFarquhar G. M., Gorodetskaya I. V., Grosvenor D. P., Lachlan-Cope T. and Van Lipzig N. P. M.: Tropospheric clouds in Antarctica, Rev. Geophys., 50(1), 2012.

Broyden C.G., A class of methods for solving nonlinear simultaneous equations, Mathematics of computation, 19, 577-593, 1965

Ceccherini S. and Ridolfi M., Technical Note: Variance-covariance matrix and averaging kernels for the Levenberg-Marquardt solution of the retrieval of atmospheric vertical profiles, Atmospheric Chemistry and Physics, 10, 3131-3139, 2010.

Choi, Y.-S., C.-H. Ho, S.-W. Kim, and R. S. Lindzen: Observational diagnosis of cloud phase in the winter antarctic atmosphere for parameterizations in climate models. Adv. Atmos. Sci., 27(6), 1233-1245, 2010, doi: 10.1007/s00376-010-9175-3.

Clough S. A.,Shephard M. W.,Mlawer E. J., Delamere J. S.,Iacono M. J.,Cady-Pereira K.,Boukabara S.,and Brown P. D., Atmospheric radiative transfer modeling: a summary of the AER codes, Short Communication, J. Quant. Spectrosc. Radiat. Transfer, 91, 233-244, 2005.

Cox, C.V., Harries J.E., Taylor J.P., Green P.D., Baran A.J., Pickering J.C., Last A.E., Murray J.E., Measurement and simulation of mid-and far-infrared spectra in the presence of cirrus, Quarterly Journal of the Royal Meteorological Society, 136 (648), 718–739, 2010.

Cox, C. J., Turner, D. D., Rowe, P. M., Shupe, M. D., Walden, V. P.: Cloud microphysical properties retrieved from downwelling infrared radiance measurements made at Eureka, Nunavut, Canada (2006-09). Journal of Applied Meteorology and Climatology, 53(3), 772–791, 2014.

Cox, C. J., Walden V. P., Rowe P. M., Shupe M. D., Humidity trends imply increased sensitivity to clouds in a warming Arctic, Nature Communication, 6, 2015.

Deeter M. N. and Evans K. F., A hybrid Eddington-single scattering radiative transfer model for computing radiances from thermally emitting atmospheres, J. Quant. Spectrosc.Radiat. Transfer 60, 4,635–648, 1998.

De Leon R. R. and Haigh D. J.,Infrared properties of cirrus clouds in climate models, Q. J. R. Meteorol. Soc. 133: 273–282 (2007).

Del Guasta M.,Morandi M. and Stefanutti L., One year of cloud lidar data from Dumont D'Urville (Antarctica) 1. General overview of geometrical and optical properties, Journal of Geophysical Research, Volume 98, No. D10, 18575-18587, 1993.

Fisher R. A., The logic of inductive inference, J.R. Stat. Soc. 98(1), 39–54 (1935).

Fu. Q., Parameterization of radiative processes in vertically nonhomogeneous multiple scattering atmospheres. PhD. dissertation, University of Utah, 259 pp. [Avalaible from University Microfilm, 305 N. Zeeb Rd, Ann Arbor,MI 48106]

Fu Q. and Liou K. N. , Parameterization of the radiative properties of cirrus clouds, J. Atmos. Sci., 50, 2008-2025, 1993.

Fu Q., An accurate parameterization of the solar radiative properties of cirrus clouds for climate models, Journal of Climate, Volume 9, 2058-2082, 1996.

Fu Q. ,Yang P., Sun W.B. , An accurate parameterization of the infrared radiative properties of cirrus clouds for climate models, American Meteorological Society, Volume 11, Issue 9, 2223-2237,1998.

Gavin H.P., The Levenberg-Marquardt method for nonlinear least squares curve-fitting problems, Department of Civil and Environmental Engineering, Duke University, (September 2015)

Hardiman S. C., Boutle I. A., Bushell A. C., Butchart, Cullen M. J. P., Field P. R., Furtado K., Manners J. C., Milton S. F., Morcrette C., O'Connor F. M., Shipway B. J., Smith C., Walters D. N., Willett M. R., Williams K. D., Wood N., Abraham N. L., Keeble J., Maycock A. C., Thuburn J., Woodhouse M. T., The Far Infrared Earth, J. Climate, 28 (16), 6516–6535, 2015.

Harries J.,Carli B. ,Rizzi R.,Serio C.,Mlynczak M.,Palchetti, L.,Maestri T.,Brindley H., and Masiello G., Processes Controlling Tropical Tropopause Temperature and Stratospheric Water Vapor in Climate Models, Reviews of Geophysics, 46, RG4004, 2008.

Heymsfield A. J.,Matrosov S.,Baum B., Ice water path-optical depth realationship for cirrus and deep stratiform ice cloud layers, American Meteorological Society, 1369–1390, 2003.

Huang, Y., S. Leroy, P. J. Gero, J. Dykema, and J. Anderson: Separation of longwave climate feedbacks from spectral observations, J. Geophys. Res., 115, D07104, 2010, doi:10.1029/2009JD012766.

Joseph J. H. and Wiscombe W. J., The delta-Eddington approximation for radiative flux transfer, Journal of the Atmospheric Sciences, 33, 2452–2459, 1976.

Kiehl J. T. and Trenberth K. E., Earth's annual global mean energy budget, Bulletin of the American Meteorological Society, Vol. 78, No. 2, 197-207, 1997.

Kahn, B. H., Irion, F. W., Dang, V. T., Manning, E. M., Nasiri, S. L., Naud, C. M., Blaisdell, J. M., Schreier, M. M., Yue, Q., Bowman, K. W., Fetzer, E. J., Hulley, G. C., Liou, K. N., Lubin, D., Ou, S. C., Susskind, J., Takano, Y., Tian, B., and Worden, J. R.: The Atmospheric Infrared Sounder version 6 cloud products, Atmos. Chem. Phys., 14, 399-426, doi:10.5194/acp-14-399-2014, 2014.

Lynch, D., Sassen, K., Star, D. O., and Sthephens G.: Cirrus, Book, Oxford University Press, Inc., 2002.

Liou, K., Influence of cirrus clouds on weather and climate processes:a global perspective, Monthly Weather Review, Volume 114, 1167-1199,1986.

Liou K. N.,Gu Y.,Yue Q., and McFarguhar G., On the correlation between ice water content and ice crystal size and its application to radiative transfer and general circulation models, Geophysical Research Letters, Vol. 35, L13805, doi:10.1029/2008GL033918, 2008.

Lubin, D., Chen B., Bromwich D. H., Somerville R. C. J., Lee W. H., and. Hines K. M.: The impact of Antarctic cloud radiative properties on a GCM climate simulation, J. Clim., 11(3), 447–462, doi:10.1175/1520-0442(1998)011<0447:TIOACR>2.0.CO;2, 1998.

Lubin D., Kahn B. H., Lazzara M. A., Rowe P. and Walden V. P.: Variability in AIRS-retrieved cloud amount and thermodynamic phase over west versus east Antarctica influenced by the SAM, Geophys. Res. Lett., 42(4), 1259–1267, 2015.

Maestri T., Rizzi R., Smith J. A., Spectral infrared analysis of a cirrus cloud based on Airborne Research Interferometer Evaluation System (ARIES) measurements, Journal of Geophysical Research: Atmospheres, 110, (D6), 2005.

Maestri, T., and Holz, R. E.: Retrieval of cloud optical properties from multiple infrared hyperspectral measurements: A methodology based on a line-by-line multiple-scattering code, IEEE Transactions on Geoscience and Remote Sensing, 47(8), 2413–2426, 2009.

Maestri T.,Rizzi R. ,Tosi E.,Veglio P.,Palchetti L.,Bianchini G.,Di Girolamo P.,Masiello G.,Serio C. ,Summa D., Analysis of cirrus cloud spectral signatures in the far infrared, J. Quant. Spectrosc. Radiat. Transfer, 141, 49–64, 2014.

Mahesh A., Walden V. P., Warren S. G.: Ground-Based Infrared Remote Sensing of Cloud Properties over the Antarctic Plateau. Part I: Cloud-Base Heights. J. Appl. Meteor., 40, 1265–1278, 2001, doi: 10.1175/1520-0450(2001)040<1265:GBIRSO>2.0.CO;2.

Mahesh A., Campbell J. R., Spinhirne J. D.: Multi-year measurements of cloud base heights at South Pole by lidar, Geo. Res. Lett., 32, L09812, doi:10.1029/2004GL021983, 2005.

Mahesh A., Walden V. P., Warren S. G.: Ground-Based Infrared Remote Sensing of Cloud Properties over the Antarctic Plateau. Part II: Cloud Optical Depths and Particle Sizes. J. Appl. Meteor., 40, 1279–1294, 2001, doi: 10.1175/1520-0450(2001)040<1279:GBIRSO>2.0.CO;2.

Marquardt D. W., An algorithm for least-squares estimation of non-linear parameters, SIAM J. Appl. Math., 11, 431-441, 1963.

Nelder J. A. and Mead R., A Simplex Method for Function Minimization, The Computer Journal, Volume 7 Issue 4, 308-313. doi: 10.1093/comjnl/7.4.308, 1965.

Palchetti L.,Bianchini G.,Castagnoli F.,Carli B.,Serio C.,Esposito F.,Cuomo V.,Rizzi R.,Maestri T., Breadboard of the Fourier transform spectrometer for the Radiation Explorer in the Far Infrared (REFIR) atmospheric mission, Applied Optics, Vol.44, No.14, pp.2870-2878, 2005.

Palchetti L.,Bianchini G.,Carli B.,Cortesi U., and Del Bianco S., Measurement of the water vapour vertical profile and of the Earth's outgoing far infrared flux, Atmos. Chem. Phys., 8, 2885–2894, 2008.

Palchetti L.,Bianchini G.,Di Natale G.,Del Guasta M., Far-Infrared radiative properties of water vapor and clouds in Antarctica, Bulletin of American Meteorological Society, http://dx.doi.org/10.1175/BAMS-D-13-00286.1 G. ,Volume 96, Issue 9, 2015.

Palchetti L.,Di Natale G., and Bianchini G., Remote sensing of cirrus microphysical properties using spectral measurements over the full range of their thermal emission, Journal of Geophysical Research, 2016.

Pithan, F., Medeiros, B., Mauritsen T.: Mixed-phase clouds cause climate model biases in Arctic wintertime temperature inversions, Clim Dyn., 43, 289, 2014, doi:10.1007/s00382-013-1964-9

Rathke C. and Fisher J., Retrieval of cloud microphysical properties from thermal infrared observations by a fast iterative radiance fitting method, Journal of atmospheric and oceanic technology, Volume 17, 1509-1524, 2000.

Remedios J. J., Leigh R. J., Waterfall A. M., Moore D. P., Sembhi H., Parkes I., Greenhough J., Chipperfield M.P., and Hauglustaine D.: MIPAS reference atmospheres and comparisons to V4.61/V4.62 MIPAS level 2 geophysical data sets, Atmos. Chem. Phys. Discuss., 7, 9973-10017, doi:10.5194/acpd-7-9973-2007, 2007.

Rodgers, C. D.: Inverse Methods for Atmospheric Sounding: Theory and Practice, World Scientific Pub Co Inc, 2000. 5559, 5580, 5581, 5589

Sassen, K., Wang, Z., Liu, D. Global distribution of cirrus clouds from CloudSat/Cloud-Aerosol lidar and infrared pathfinder satellite observations (CALIPSO) measurements, Journal of Geophysical Research - Atmospheres, 113(D8), 2008.

Scott, R. C., and D. Lubin: Unique manifestations of mixed-phase cloud microphysics over Ross Island and the Ross Ice Shelf, Antarctica, Geophys. Res. Lett., 43, 2936–2945, 2015, doi:10.1002/2015GL067246

Stocker, T. F., et al., IPCC, 2013: climate change 2013: the physical science basis. Contribution of working group I to the fifth assessment report of the intergovernmental panel on climate change, Cambridge University Press, 2013.

Turner D.D., Arctic Mixed-Phase Cloud Properties from AERI Lidar Observations: Algorithm and Results from SHEBA, Journalof Applied Meteorology, Vol. 44, 427-444, 2005.

Turner D.D.,Ackerman S.A.,Baum B.A.,Revercomb H.E.,Yang P., Cloud Phase Determination Using Ground-Based AERI Observations at SHEBA, Journal of Applied Meteorology, Vol. 42, 710−715, 2003.

Vömel H.,Selkirk H.,Miloshevich L,Valverde-Canossa J.,Valdès J.,Kyrö E.,Kivi R.,Stolz W.,Peng G., and Diaz J. A., Radiation Dry Bias of the Vaisala RS92 Humidity Sensor, Journal of atmospheric and oceanic technology, Volume 24, 953-963, 2007.

Yang P.,Gao B. C.,Baum B. A.,Hu Y. X. ,Wiscombe W. J.,Tsay S. C., Winker D. M., and Nasiri S. L., Radiative properties of cirrus clouds in the infrared (8 – 13 mm) spectral region, J. Quant. Spectrosc. Radiat.Transfer, 70, 473 – 504, 2001.

Yang P., Wei H.,Huang H.-L. ,Baum B. A.,Hu Y. X.,Kattawar G. W.,Mishchenko M. I., and Fu Q. , Scattering and absorption property database for nonspherical ice particles in the near-through far-infrared spectral region, Applied Optics, 44, 26 (2005).

Wild M.,Folini D.,C. Schär C.,Loeb N.,Dutton E. G.,König-Langlo G., The global energy balance from a surface perspective, Clim Dyn (2013) 40:3107–3134 DOI 10.1007/s00382-012-1569-8

Wylie D. P. and Menzel W. P.: Eight Years of High Cloud Statistics Using HIRS, J. Climate, 12(1), 170–184, 1999.

Wiser K. and Yang P., Average ice crystal size and bulk short-wave single-scattering properties of cirrus clouds, Atmospheric Research 49 (1998) 315–335.

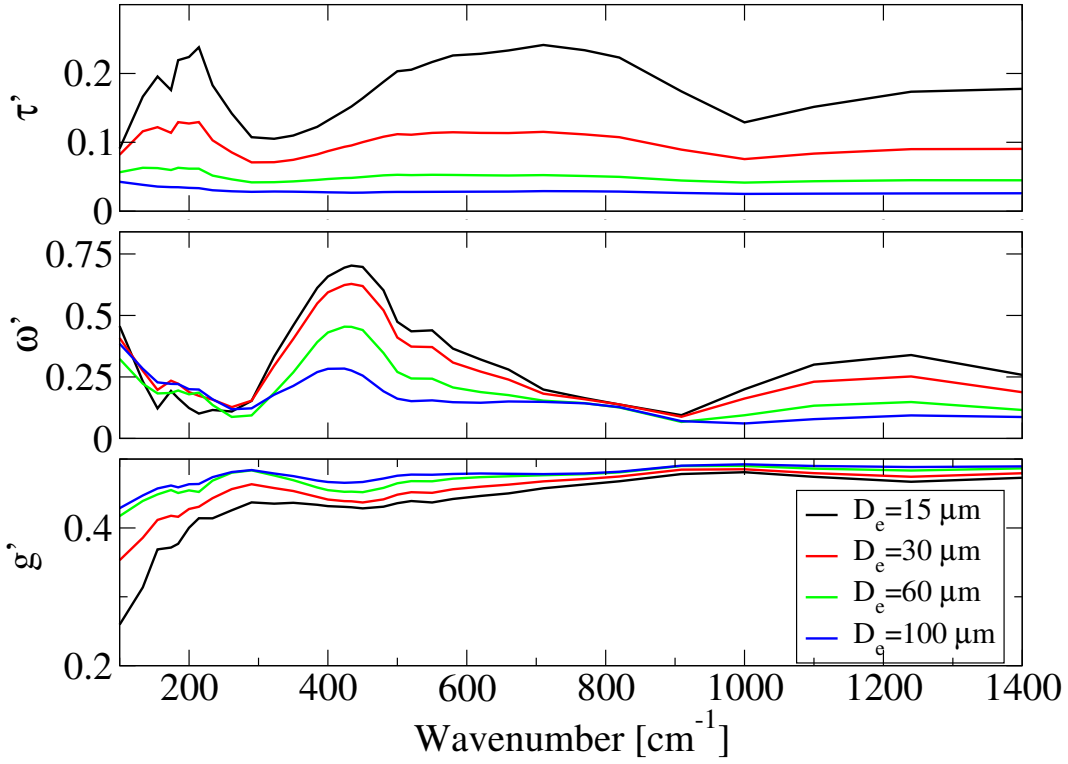

Figure 1. Scaled optical parameters for different values of D_{ge}. The optical depth τ is calculated for IWP=2 gm^{-2}.

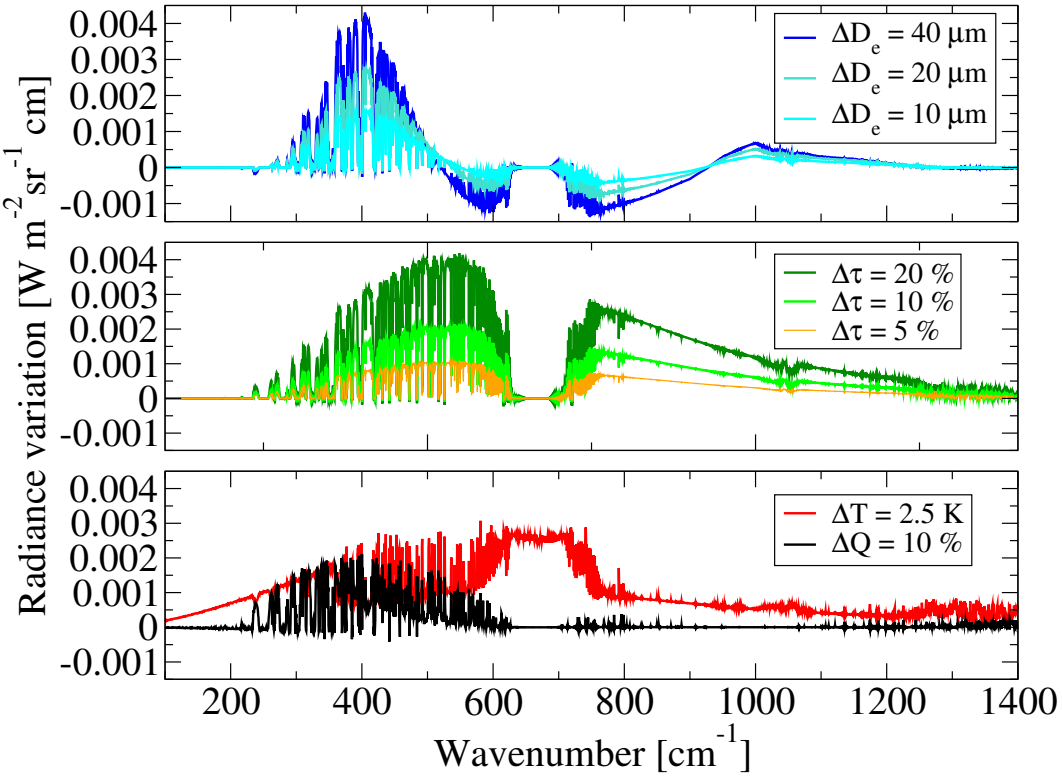

Figure 2. Radiance sensitivity to parameter variation for a summer atmospheric state and a cirrus cloud of 1 km with the bottom at 1800 m above ground, τ = 1, and D_e = 40 μm.

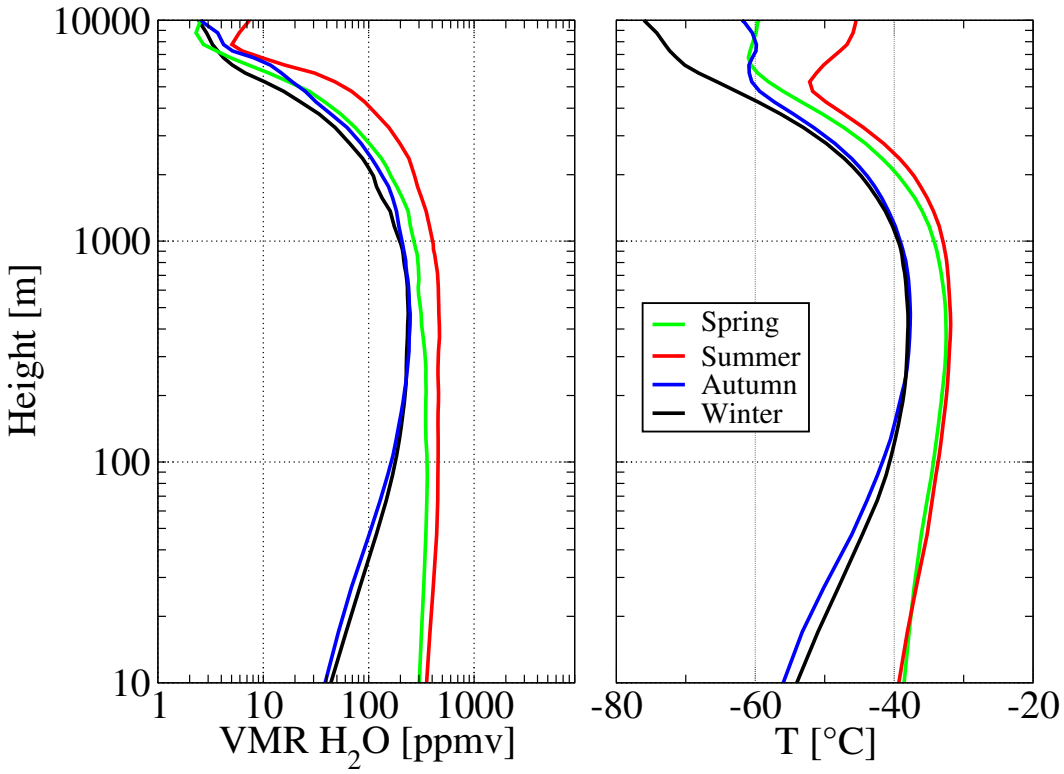

Figure 3. Plotting of the four seasonal climatological profiles of water vapour VMR (left panel) and temperature (right panel) used as initial guesses in the fitting procedure.

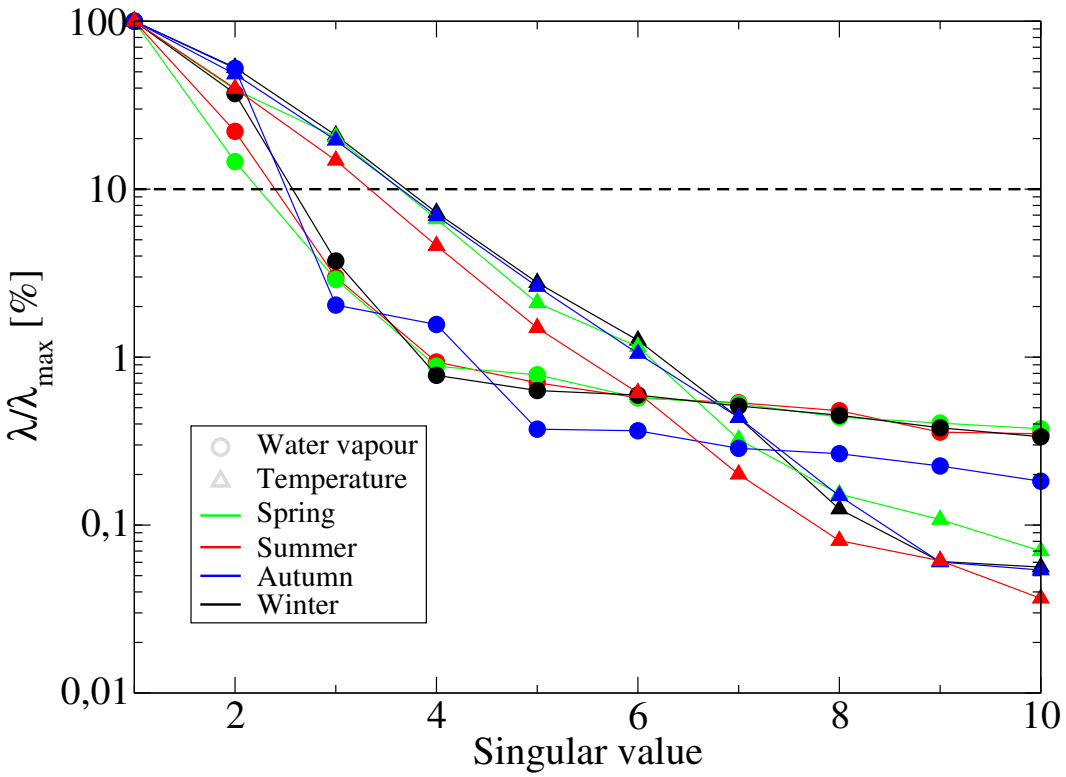

Figure 4. Trend of the ratios between the singular values and the maximum for water vapour (circles) as well as the temperature (triangles) are reported in percentage for every season (different colours). The threshold of the singular independent states represented by the black-dashed line, identifies the limit value used in this analysis.

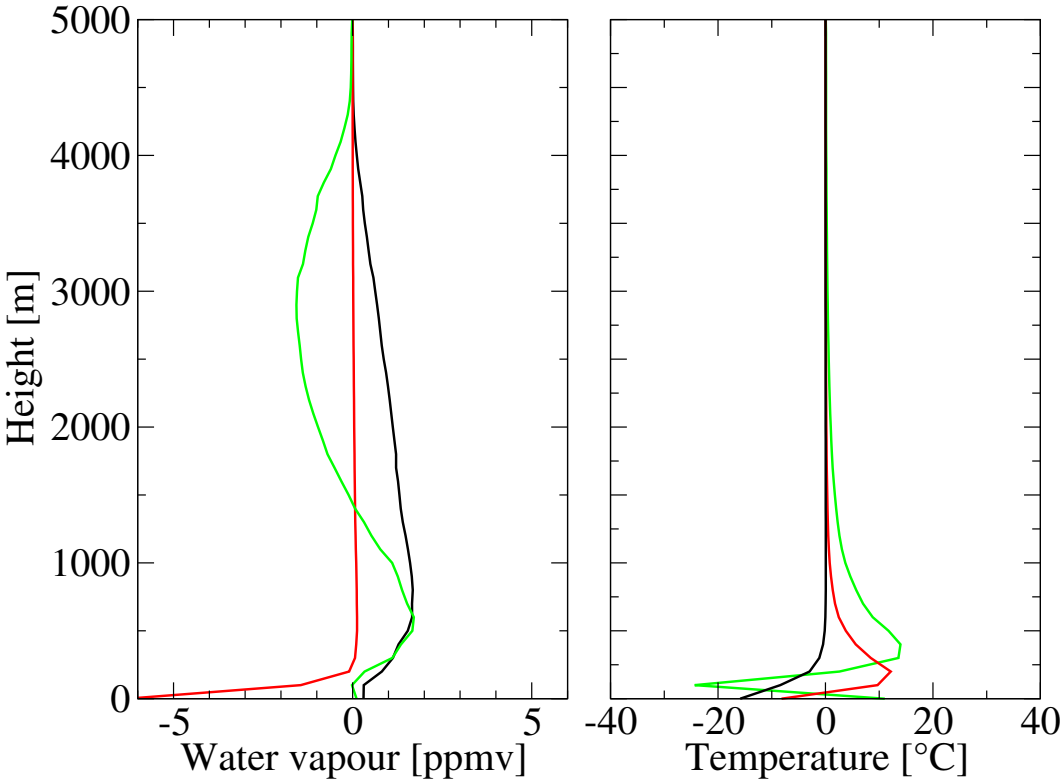

Figure 5. First back-transformed singular vectors of $\widetilde{\mathbf{K}}$ of water vapour and temperature for the singular values greater than about 10 % of the maximum calculated by using the winter climatology.

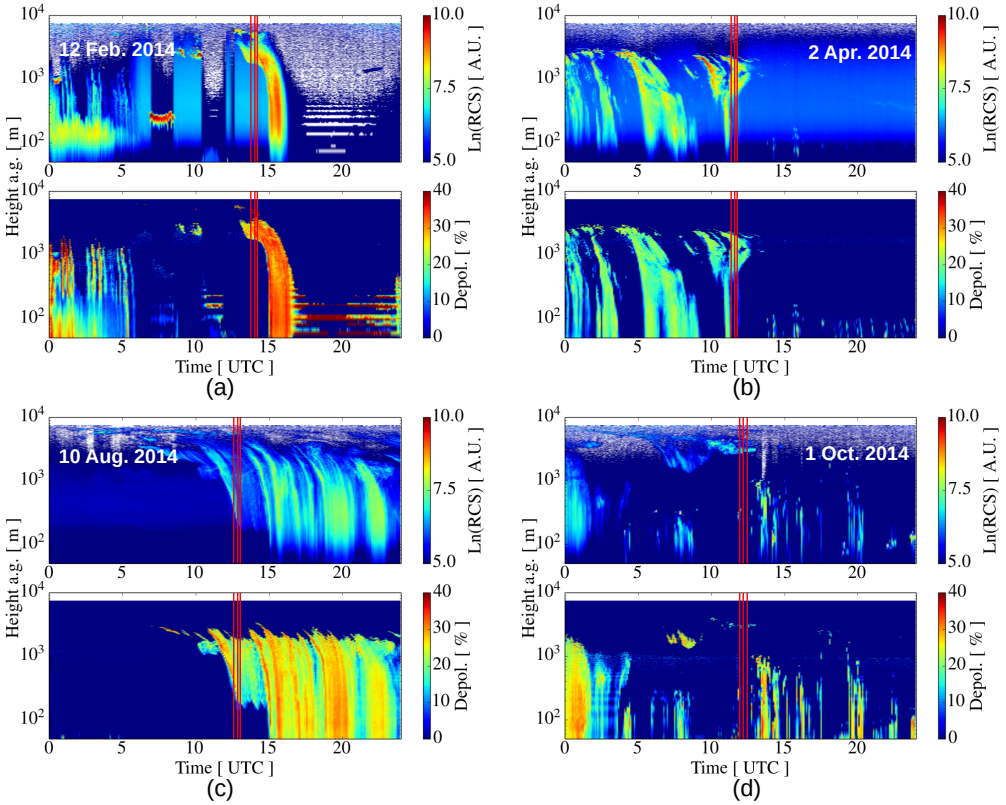

Figure 6. Colour maps of RCS and depolarisation signals performed by the lidar at Dome-C for different days and seasons. The panels show the passage of an ice cloud in Summer on 12 February 2014 (a), in Autumn on 2 April 2014 (b), in Winter on 10 August 2014 (c), and in Spring on 1 October 2014 (d). The red lines indicate the times at which the analysed spectra were acquired.

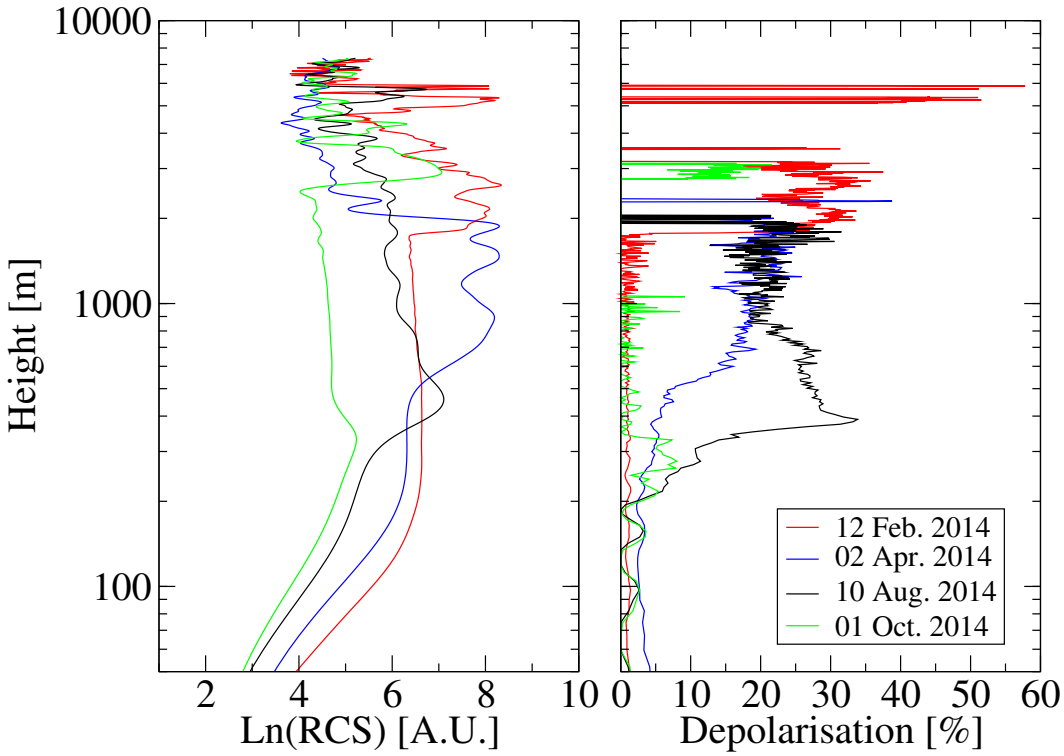

Figure 7. Logarithmic RCS and depolarisation signal corresponding to the four selected days in coincidence with the measurements nearest to 12 UTC.

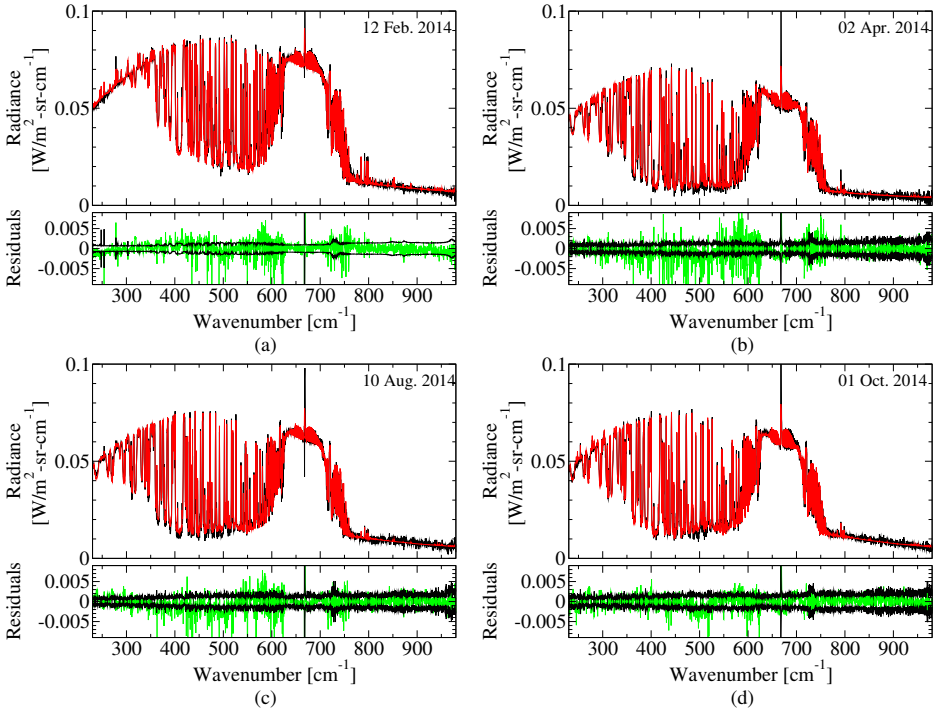

Figure 8. Comparisons of the synthetic spectra (red) provided by the retrieval with the measurements (black) nearest to 12 UTC for the same days shown in Fig. 6. The lower panels show the comparisons of the residuals (green) with the measurement uncertainty.

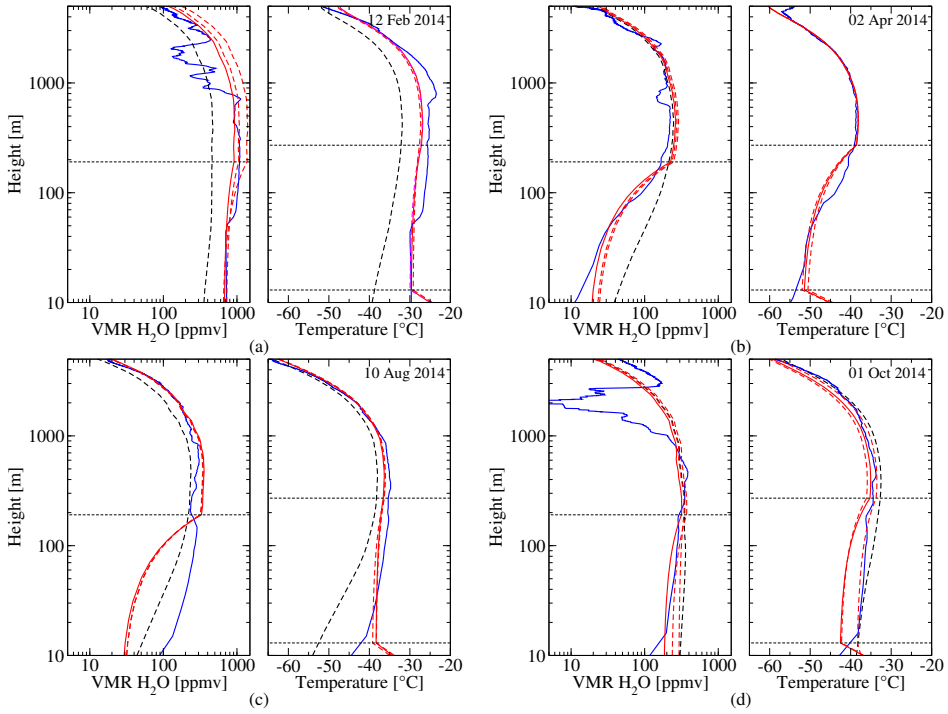

Figure 9. Comparison of the retrieved profiles of water vapour VMR and temperature for the selected measurements (red continuous and dashed lines) of Fig. 8 with the 12-UTC radiosounding profiles (blue line) and the initial guess (dashed black line). The red continuous lines are related to the profile with better temporal coincidence with the radiosounding.

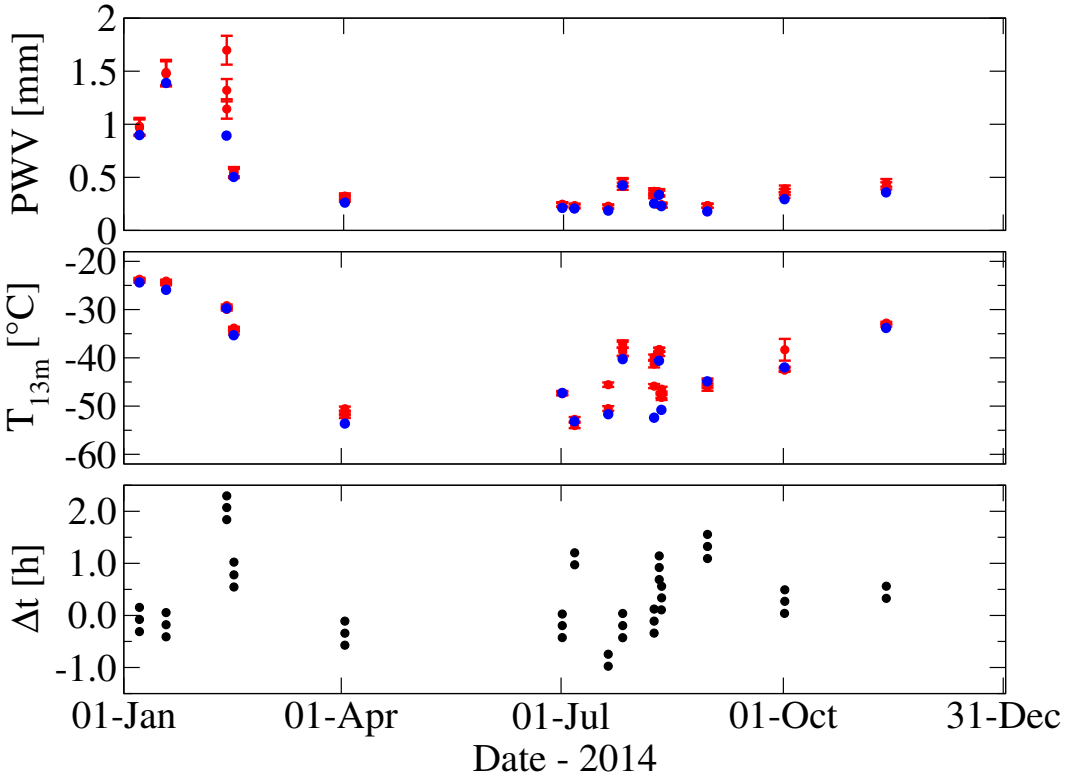

Figure 10. Comparison between the retrieved PWV and temperature of the level at 13 m above ground (red) compared with the corresponding radiosonde values (blue). The bottom panel shows the time difference between the retrieved parameters and the nearest radiosonde profiles used for the comparison.

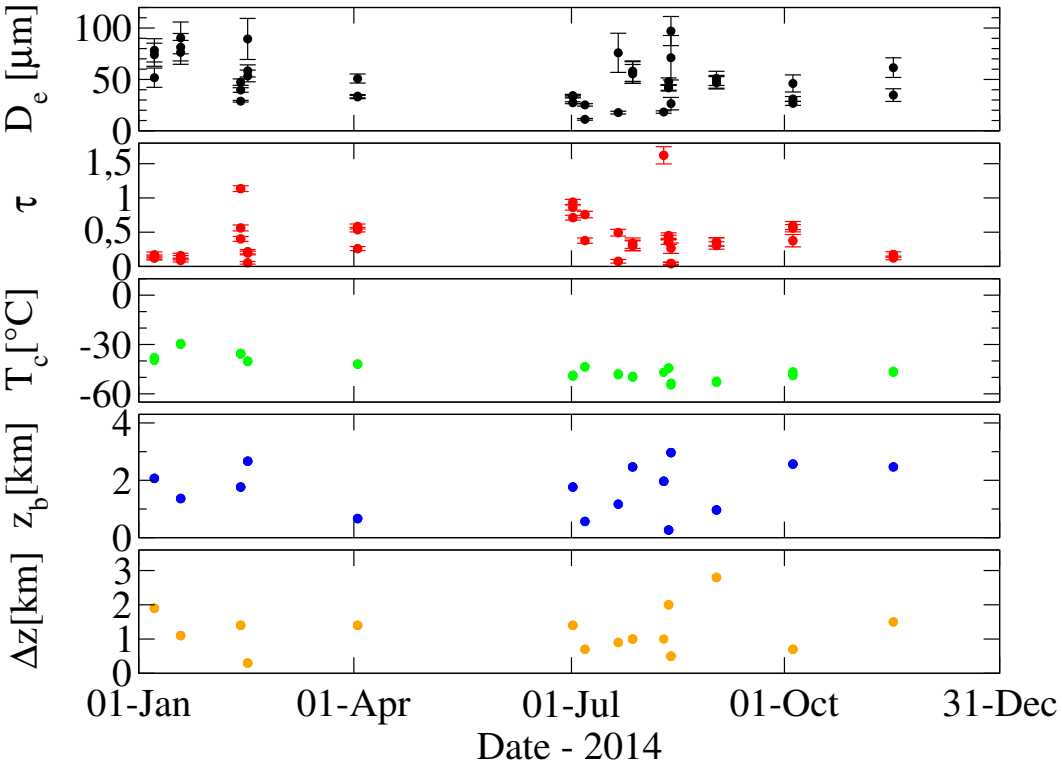

Figure 11. Time evolution of the retrieved clouds parameters: the generalised effective diameter D_e, optical depth τ, the cloud temperature T_c. The cloud bottom height z_b and the thickness Δz are also shown.

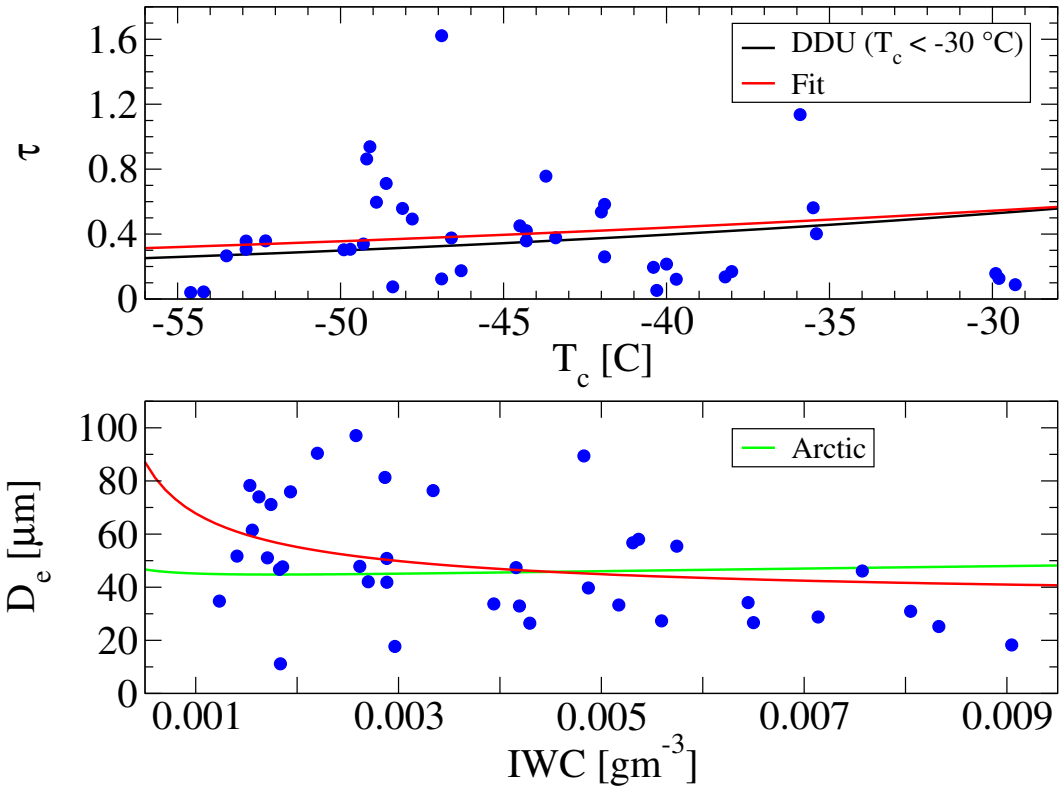

Figure 12. Retrieved data (blue dots) and fit (red line) of optical depth as a function of temperature are compared with the Dumont D'Urville (DDU) statistics (black line) in the upper panel and with the Arctic $D_e - \mathrm{IWC}$ distribution (Liou, 2008) (green line) in the lower panel.